


Article

Surface Aggregation Adsorption of Binary Solutions Between Diiodomethane, Furfural, and *N,N*-Dimethylformamide

Zhongwei Huang ¹, Na Du ¹  and Wanguo Hou ^{1,2,*}

¹ Key Laboratory of Colloid & Interface Chemistry (Ministry of Education), Shandong University, Jinan 250100, China; 202312139@mail.sdu.edu.cn (Z.H.); duna@sdu.edu.cn (N.D.)

² National Engineering Technology Research Center of Colloidal Materials, Shandong University, Jinan 250100, China

* Correspondence: wghou@sdu.edu.cn; Tel.: +86-531-88365460; Fax: +86-531-88364750

Abstract

The surface tensions (σ) of binary solutions of diiodomethane (DIM, 1)–furfural (FA, 2), DIM (1)–*N,N*-dimethylformamide (DMF, 2), and FA (1)–DMF (2) were determined at 25 °C over the entire bulk composition range, and the surface adsorption behavior was analyzed using the surface aggregation adsorption (SAA) model proposed recently. In particular, by combining the SAA model with the Gibbs adsorption equation, the changes in the Gibbs surface excess (Γ_2) and the adsorption layer thickness (τ) with the bulk composition ($x_{2,b}$) were investigated. The SAA model combined with the modified Eberhart model can well describe the σ -isotherms of the three binary solutions. The surface adsorption trends of component 2 in DIM–FA, DIM–DMF, and FA–DMF decrease in turn. The change trends of Γ_2 and τ with $x_{2,b}$ are dependent on the SAA model parameters, namely, the adsorption equilibrium constant (K_x) and the average aggregation number (n). With an increase in $x_{2,b}$, Γ_2 continuously increases when $K_x < 2v_1/[n(2n - 1)v_2]$ (where v_1 and v_2 are the partial molar volumes of components 1 and 2, respectively); otherwise (i.e., $K_x \geq 2v_1/[n(2n - 1)v_2]$), Γ_2 initially increases and then decreases, showing a maximum on the Γ_2 -isotherm. When $n \geq 1$, τ gradually decreases with an increase in $x_{2,b}$; otherwise (i.e., $n < 1$), τ initially increases and then decreases, showing a maximum on the τ -isotherm. An increase in the adsorption trend leads to a decrease in both Γ_2 and τ . This work provides a better understanding of the surface adsorption behavior of liquid mixtures.

Keywords: liquid mixture; surface adsorption; surface aggregation; adsorption layer thickness; thermodynamic model



Academic Editor: Reinhard Miller

Received: 12 September 2025

Revised: 29 September 2025

Accepted: 2 October 2025

Published: 9 October 2025

Citation: Huang, Z.; Du, N.; Hou, W.

Surface Aggregation Adsorption of Binary Solutions Between Diiodomethane, Furfural, and *N,N*-Dimethylformamide. *Colloids Interfaces* **2025**, *9*, 67. <https://doi.org/10.3390/colloids9050067>

Copyright: © 2025 by the authors. Licensee MDPI, Basel, Switzerland. This article is an open access article distributed under the terms and conditions of the Creative Commons Attribution (CC BY) license (<https://creativecommons.org/licenses/by/4.0/>).

1. Introduction

Surface adsorption of liquid mixtures is an important interfacial phenomenon [1–4], which involves three fundamental physical quantities, namely, the surface tension, composition, and thickness of surface adsorption layers. Many techniques, such as ellipsometry [5,6], neutron reflection [7,8], mass spectrometry (combined with an indigenous cluster beam apparatus) [9], vibrational frequency spectroscopy [10,11], and metastable induced electron spectroscopy [12], have been used to determine the composition and thickness of surface layers, but it is currently difficult to accurately (or independently) obtain data over the entire composition range. Owing to the fact that the surface tension of liquid mixtures is easy to accurately determine over the entire composition range, thermodynamic models are typically used to predict (or estimate) the composition and thickness of surface layers from the surface tension data [8,13–21].

Many thermodynamic (or empirical or semi-empirical) models have been developed to relate the surface properties (tension, composition, and thickness) of liquid mixtures with their bulk compositions [22–35]. However, due to the complexity of surface phenomena, existing models still lack universality [33,34]. For instance, the surface tension isotherms of binary solutions can be divided into two main types, namely, the Langmuir-type (L-type) and the sigmoid-type (S-type) [33]. Most of the existing models can reasonably describe the L-type isotherms, but not the S-type ones [33]. This is because some assumptions in establishing the models deviate from the real state of solutions. In fact, the dependence of the surface composition and thickness on the bulk composition is still not fully understood.

Recently, we proposed a thermodynamic model, called the “surface aggregation adsorption” (SAA) model, for liquid mixtures, relating the surface composition with the bulk one [33,34]. By coupling it with the modified Eberhart model [25,28], an equation with two parameters (i.e., the adsorption equilibrium constant and the average aggregation number) was developed to relate the surface tension with the bulk composition, which can well describe the L-type and S-type isotherms [33]. In addition, the SAA model and the modified Eberhart model can be combined with the Gibbs adsorption equation to calculate the Gibbs excess and thickness of adsorption layers [36]. Previous reports on the change in surface layer thicknesses with bulk compositions mainly focused on the aqueous solutions of short-chain alcohols (especially ethanol) [8–10,13,17,18,36], but yet no reports on non-aqueous solutions. It is interesting to understand the dependence of the thickness of surface adsorption layers (or the Gibbs excess layers) on the bulk composition.

In the current work, the surface tensions (σ) of binary solutions between diiodomethane (DIM), furfural (FA), and *N,N*-dimethylformamide (DMF) were determined over the entire bulk composition range, and the surface adsorption behavior was analyzed using the SAA model from the σ data. In particular, by combining the SAA model and the modified Eberhart model with the Gibbs equation, the changes in the Gibbs excess and thickness of the adsorption layer with the bulk composition were investigated. This work provides a better understanding of the surface adsorption behavior of liquid mixtures.

2. Experimental Section and Theoretical Basis

2.1. Chemicals

Diiodomethane (DIM) was purchased from Aladdin (Shanghai, China). Furfural (FA) and *N,N*-dimethylformamide (DMF) were purchased from Macklin (Shanghai, China). All chemicals were of analytical grade and used as received. Ultrapure water (with a resistivity of 18.25 M Ω ·cm at 25.0 °C) was obtained using a Hitech-Kflow water purification system (Hitech, Shanghai, China).

2.2. Surface Tension Determination

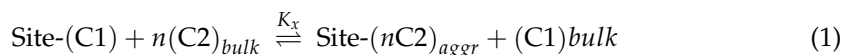
Surface tensions of pure liquids (σ_0) and their mixtures (σ) were measured at 25.0 \pm 0.2 °C using a Sigma 700 automatic tensiometer (Biolin, Gothenburg, Sweden). Each test sample was equilibrated for at least 10 min before measurements. All of the tests were performed in triplicate, and their average values were reported here.

2.3. Theoretical Basis

For clarity, the theoretical basis of the SAA model [33] and the surface excess model are summarized in the following.

Let us consider a binary solution consisting of components 1 and 2, with a planar surface layer. The surface layer is considered as a homogeneous surface phase with a definite thickness (τ) [20,24–27,29–34].

The SAA model. The SAA model [33] assumes that: (1) the molecules of component 2 (commonly the surface-active component) adsorb into the surface layer, directly forming aggregates with an average aggregation number of n , and (2) the surface layer consists of surface sites, and each site is occupied by one molecule of component 1 or one aggregate formed by component 2. The adsorption equilibrium is schematically expressed as



where Site represents the surface sites, (C1) and (C2) represent the molecules of components 1 and 2, respectively, $(n\text{C2})_{\text{aggr}}$ represents an aggregate formed by n molecules of component 2, the subscript “bulk” represents the bulk phase, and K_x is the adsorption equilibrium constant.

Further, assume that the activity coefficients of all of the species Site-(C1), Site-($n\text{C2})_{\text{aggr}}$, $(\text{C1})_{\text{bulk}}$, and $(\text{C2})_{\text{bulk}}$ are unity. According to the adsorption equilibrium principle, the K_x can be expressed as,

$$K_x = \frac{x_{\text{aggr}} x_{1,\text{b}}}{x_{1,\text{s}} x_{2,\text{b}}^n} \quad (2)$$

where x_{aggr} and $x_{1,\text{s}}$ are the mole fractions of aggregates and component 1 in the surface phase, respectively, and $x_{1,\text{b}}$ and $x_{2,\text{b}}$ are the mole fractions of components 1 and 2 in the bulk phase, respectively.

Assuming that the partial molar volume of aggregates (v_{aggr}) equals n times that of component 2 in the surface phase ($v_{2,\text{s}}$), i.e., $v_{\text{aggr}} = nv_{2,\text{s}}$, Equation (2) can be written as

$$K_x^* = \frac{\phi_{2,\text{s}} x_{1,\text{b}}}{\phi_{1,\text{s}} x_{2,\text{b}}^n} \quad (3)$$

where $\phi_{1,\text{s}}$ and $\phi_{2,\text{s}}$ are the volume fractions of components 1 and 2 in the surface phase, and $K_x^* \equiv nv_{2,\text{s}}K_x/v_{1,\text{s}}$, here $v_{1,\text{s}}$ is the partial molar volume of component 1 in the surface phase.

Considering $\phi_{1,\text{s}} + \phi_{2,\text{s}} = 1$ and $x_{1,\text{b}} + x_{2,\text{b}} = 1$, from Equation (3) one has

$$\phi_{2,\text{s}} = \frac{K_x^* x_{2,\text{b}}^n}{1 - x_{2,\text{b}} + K_x^* x_{2,\text{b}}^n} \quad (4)$$

Equation (4) is the SAA model equation. If $n = 1$, Equation (4) becomes the Langmuir-like model [33,37].

Since the surface compositions are now difficult to determine, the estimation of the two parameters (K_x and n) requires another independent equation that connects the surface compositions with the surface tension. A suitable and widely used equation is the modified Eberhart mixing rule [25,28], which is represented as

$$\sigma = \phi_{1,\text{s}} \sigma_1^0 + \phi_{2,\text{s}} \sigma_2^0 \quad (5)$$

where σ is the surface tension of binary liquid mixtures, and σ_1^0 and σ_2^0 are the surface tensions of pure components 1 and 2, respectively. Equation (5) gives $\pi_r = \phi_{2,\text{s}}$, where π_r is the reduced surface pressure (π_r) [27], defined as $\pi_r = (\sigma_1^0 - \sigma)/(\sigma_1^0 - \sigma_2^0)$. According to Equation (5), the surface composition can be obtained only from σ data.

Combining Equations (4) and (5) gives

$$\sigma = \sigma_1^0 - \frac{K_x^* x_{2,\text{b}}^n}{x_{1,\text{b}} + K_x^* x_{2,\text{b}}^n} (\sigma_1^0 - \sigma_2^0) \quad (6)$$

$$\pi_r = \frac{K_x^* x_{2,b}^n}{1 - x_{2,b} + K_x^* x_{2,b}^n} \quad (7)$$

Equation (7) can be written in a linear form as

$$\lg \frac{\pi_r(1 - x_{2,b})}{1 - \pi_r} = \lg K_x^* + n \lg x_{2,b} \quad (8)$$

Equation (8) indicates that the plot of $\lg[\pi_r(1 - x_{2,b})/(1 - \pi_r)]$ vs. $\lg x_{2,b}$ should be a straight line, and the values of n and K_x^* (and thus K_x) can be estimated from its slope and intercept.

Adsorption free energy. Based on the adsorption equilibrium principle, the standard Gibbs free energy change in adsorption per mole of component 2 (ΔG_{ad}^0) can be represented as [33]

$$\Delta G_{ad}^0 = -\frac{RT}{n} \ln K_x \quad (9)$$

where R is the universal gas constant and T is the absolute temperature. Equation (9) indicates that the adsorption tendency is determined by K_x and n . For positive adsorption ($K_x > 1$ and $\Delta G_{ad}^0 < 0$), larger K_x and smaller n correspond to a stronger adsorption tendency (i.e., a larger $|\Delta G_{ad}^0|$).

The surface excess. The surface excess (or adsorption amount) is a relative quantity characterizing the difference in compositions between the surface phase and the bulk phase. There exist different definitions for the surface excess [24], among which the most widely used is the Gibbs surface excess.

At constant T and pressure (p), and assuming the activity coefficients of all components being unity, the Gibbs adsorption equation can be expressed as [1]

$$\Gamma_2 = -\frac{x_{2,b}}{RT} \frac{d\sigma}{dx_{2,b}} \quad (10)$$

where Γ_2 is the Gibbs surface excess of component 2, defined by the Gibbs dividing surface (a zero-volume dividing surface within the surface layer, located at the position with zero surface excess of component 1) [1]. Guggenheim and Adam [24] elucidated the physical meaning of the Gibbs excess, i.e., the difference between the amount of adsorbate (here component 2) contained in the adsorbed layer per unit area and that contained in the bulk solution with the same amount of solvent (here component 1) as the adsorbed layer [13,16,17].

Combining Equation (10) with Equation (6) gives,

$$\Gamma_2 = \frac{K_x^* x_{2,b}^n (n x_{1,b} + x_{2,b})}{RT (x_{1,b} + K_x^* x_{2,b}^n)^2} (\sigma_1^0 - \sigma_2^0) \quad (11)$$

This is the algebraic expression for the Gibbs surface excess, which can be used to calculate Γ_2 over the entire concentration range ($x_{2,b} = 0-1$) with the parameters K_x^* and n obtained from the SAA model. For simplicity, Equation (11) may be called the Gibbs-SAA equation.

From Equation (11), the limiting values of Γ_2 at $x_{2,b} \rightarrow 0$ and $x_{2,b} \rightarrow 1$, denoted as $\Gamma_{2(x \rightarrow 0)}$ and $\Gamma_{2(x \rightarrow 1)}$, respectively, can be obtained as

$$\lim_{x_{2,b} \rightarrow 0} \Gamma_2 \equiv \Gamma_{2(x \rightarrow 0)} = 0 \quad (12)$$

$$\lim_{x_{2,b} \rightarrow 1} \Gamma_2 \equiv \Gamma_{2(x \rightarrow 1)} = \frac{1}{RT K_x^*} (\sigma_1^0 - \sigma_2^0) \quad (13)$$

At $x_{2,b} \rightarrow 0$, $\Gamma_2 = 0$, an expected result; while at $x_{2,b} \rightarrow 1$, $\Gamma_2 > 0$ (i.e., $\Gamma_2 \neq 0$), arising from the definition (or physical meaning) of the Gibbs surface excess [1,22,24]. A strong adsorption trend (i.e., large K_x^* or K_x) results in a low $\Gamma_{2(x \rightarrow 1)}$. Over the entire concentration range ($x_{2,b} = 0-1$), $\Gamma_2 \geq 0$, indicating positive adsorption of component 2 with lower surface tension ($\sigma_2^0 < \sigma_1^0$).

In addition, the surface excess can be expressed by the difference in the absolute concentrations between the surface and bulk phases, called “the absolute surface excess”:

$$\Delta\Phi_2 = \phi_{2,s} - \phi_{2,b} \quad (14)$$

$$\Delta X_2 = x_{2,s} - x_{2,b} \quad (15)$$

where $\Delta\Phi_2$ and ΔX_2 are the surface excess expressed by the mole and volume fractions, respectively, for component 2.

Adsorption layer thickness. Based on the Gibbs equation and the SAA model, an equation for predicting the adsorption layer thickness τ can be established [36]. According to the physical meaning of the Gibbs excess Γ_2 [1,24], one has,

$$\Gamma_2 = \frac{\tau}{v_2} \left(\phi_{2,s} - \frac{\phi_{1,s}}{\phi_{1,b}} \phi_{2,b} \right) \quad (16)$$

Note that the term in the bracket is the Gibbs surface excess expressed in volume fraction (defined by the Gibbs dividing surface). Let $\Delta\Phi_2^{(1)} \equiv \phi_{2,s} - \phi_{1,s} \phi_{2,b} / \phi_{1,b}$. The $\Delta\Phi_2^{(1)}$ values can be calculated using the modified Eberhart mixing rule Equation (5) from the σ data. At $\phi_{2,b} \rightarrow 1$ (or $x_{2,b} \rightarrow 1$), one has

$$\lim_{x_{2,b} \rightarrow 1} \Delta\Phi_2^{(1)} \equiv \Delta\Phi_{2(x \rightarrow 1)}^{(1)} = 1 - \frac{1}{nK_x} \quad (17)$$

Strong adsorption trends (large nK_x) lead to large $\Delta\Phi_{2(x \rightarrow 1)}^{(1)}$. If $nK_x = 1$ (or $n = 1$ and $K_x = 1$), $\Delta\Phi_{2(x \rightarrow 1)}^{(1)} = 0$, corresponding to the ideal state.

Combining Equation (16) with Equations (3), (4), and (11) gives

$$\tau = \frac{v_{1,s} v_{2,s} n K_x (n x_{1,b} + x_{2,b})}{RT (v_{1,s} x_{1,b} + v_{2,s} n K_x x_{2,b}^n) (n K_x - x_{2,b}^{1-n})} (\sigma_1^0 - \sigma_2^0) \quad (18)$$

Equation (18) is the adsorption layer thickness (ALT) equation, which can predict τ over the entire bulk concentration range. Note that the physical meaning of the so-obtained τ is the thickness of the surface excess layer, rather than that of the “real” surface layer of liquids. The thickness of the surface excess layer is determined only by its composition difference with the bulk phase, while that of the “real” surface layer is determined by all physical properties different from the bulk phase (such as density besides composition [6]).

If $K_x = 1$ and $n = 1$, Equation (18) gives $\tau \rightarrow \infty$, which is reasonable, because the condition ($K_x = 1$ and $n = 1$) corresponds to the “ideal” state, i.e., no surface adsorption occurs (with $\tau \rightarrow \infty$ or $\tau = 0$). It should be noted that, for the binary systems with $n \leq 1$, the ALT equation is applicable over the entire $x_{2,b}$ range, but for those with $n > 1$, it gives unreasonable (negative or infinite) τ at extremely low $x_{2,b}$ (i.e., when $x_{2,b} \leq (1/nK_x)^{1/(n-1)}$). For example, for a binary system with $n = 1.27$ and $K_x = 6.37$ (corresponding to the DIM-FA system, see Section 3.1), Equation (18) gives negative or infinite τ at $x_{2,b} \leq 4.3 \times 10^{-4}$. When $K_x > 1$ and $n > 1$, the σ -isotherm is S-type [33]. That is, Equation (18) is not fully applicable to systems with S-type isotherms. This is because the modified Eberhart mixing rule Equation (5) is an empirical equation [29], not a thermodynamic one. It can be seen from Equation (16) that if Equation (5) gives $\Delta\Phi_2^{(1)} \leq 0$ while the Gibbs equation (Equation (10)) gives $\Gamma_2 > 0$,

an unreasonable negative or infinite τ will be obtained. In fact, a more reasonable scenario is that, at $x_{2,b} \rightarrow 0$ (or $\phi_{2,s} \rightarrow 0$), no surface aggregation occurs, i.e., $n = 1$ (rather than $n > 1$). Therefore, for the systems with $n > 1$, the τ at extremely low $x_{2,b}$ can be estimated by extrapolating τ at $x_{2,b} > (1/nK_x)^{1/(n-1)}$ to $x_{2,b} = 0$.

From Equation (18), the limiting τ values at $x_{2,b} \rightarrow 0$ (with $n \leq 1$) and $x_{2,b} \rightarrow 1$, denoted as $\tau_{x \rightarrow 0}$ and $\tau_{x \rightarrow 1}$, respectively, can be obtained as

$$\lim_{x \rightarrow 0} \tau \equiv \tau_{x \rightarrow 0} = \frac{v_{2,s}K_x}{RT(K_x - 1)} (\sigma_1^0 - \sigma_2^0) \quad (\text{for } n = 1) \quad (19)$$

$$\lim_{x \rightarrow 0} \tau \equiv \tau_{x \rightarrow 0} = \frac{v_{2,s}n}{RT} (\sigma_1^0 - \sigma_2^0) \quad (\text{for } n < 1) \quad (20)$$

$$\lim_{x \rightarrow 1} \tau \equiv \tau_{x \rightarrow 1} = \frac{v_{1,s}}{RT(nK_x - 1)} (\sigma_1^0 - \sigma_2^0) \quad (21)$$

Equations (19)–(21) indicate that strong adsorption trend (i.e., large K_x and low n) results in small $\tau_{x \rightarrow 0}$ and $\tau_{x \rightarrow 1}$, similar to the case of $\Gamma_{2(x \rightarrow 1)}$. In addition, $\tau_{x \rightarrow 0}$ is related to $v_{2,s}$ while $\tau_{x \rightarrow 1}$ to $v_{1,s}$, which are consistent with the physical meaning of τ thus obtained.

2.4. Model Fitting

The model fitting for test data was performed using Origin2016 software with the Levenberg–Marquardt algorithm. The best-fit values of model parameters were automatically obtained from the software, which correspond to the minimum sum of squares of residuals. The average absolute deviation (AAD) and the average relative deviation (ARD) were used as accuracy criteria, which are represented as

$$\text{AAD} = \frac{1}{m} \sum_{i=1}^m |X_{\text{exp}} - X_{\text{cal}}| \quad (22)$$

$$\text{ARD} = \frac{100\%}{m} \sum_{i=1}^m \frac{|X_{\text{exp}} - X_{\text{cal}}|}{X_{\text{exp}}} \quad (23)$$

where X_{exp} and X_{cal} are the experimental and model-calculated values of the physical quantity X , and m represents the number of data points. Low AAD and ARD values indicate that the model fits the experimental data well.

3. Results and Discussion

Based on the SAA model, the Gibbs-SAA equation, and the ALT equation, we investigated the surface adsorption behavior of three binary solutions: DIM (1)–FA (2), DIM (1)–DMF (2), and FA (1)–DMF (2). Table 1 shows the physical properties of pure liquids (DIM, FA, and DMF) involved here, including their relative molar masses (M_r), densities (ρ^0 , at 25 °C) and critical densities (ρ_c^0) [38]. Their bulk molar volumes (v_b^0 , at 25 °C) and critical molar volumes (v_c^0) were calculated using M_r , ρ^0 , and ρ_c^0 , which are also listed in Table 1. Note that the v_c^0 and ρ_c^0 values of DIM were estimated using the Wetere method [38]. The surface tensions (σ^0) of the pure liquids DIM, FA, and DMF were determined here at 25 °C to be 49.04, 43.10, and 36.40 mN/m, respectively, which are very close to the literature-reported values (ca. 50.0–50.55, 43.0–43.10, and 36.52–36.98 mN/m, respectively) [38–46], indicating that the σ data determined here are credible.

Table 1. Physical properties of pure liquids.

Liquid	M_r (g/mol)	ρ^0 (g/cm ³)	ρ_c^0 (g/cm ³)	v_b^0 (cm ³ /mol)	v_c^0 (cm ³ /mol)	v_s^0 (cm ³ /mol)	l_s (nm)
DIM	267.84	3.33	~0.91	80.43	~297	176.1	0.66
FA	96.09	1.16	0.359	82.84	267.6	167.4	0.65
DMF	73.10	0.94	0.267	77.77	273.7	165.5	0.65

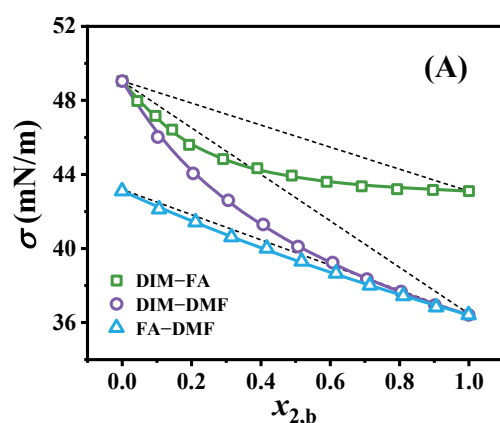
In the following model calculations, let $v_{1,s}/v_{2,s} = v_{1,b}/v_{2,b}$ and assume the partial molar volume of component i is equal to its molar volume ($v_i = v_i^0$) [22]. In addition, assume that the amount of matter of the surface phase is significantly lower than that of the bulk phase, that is, the surface adsorption does not induce a change in the bulk composition [21].

3.1. Surface Aggregation Adsorption

The surface tensions of DIM (1)–FA (2), DIM (1)–DMF (2), and FA (1)–DMF (2) binary solutions were determined at 25.0 °C over the entire $x_{2,b}$ range. The σ and π_r data are shown in Tables S1–S3 in the Supporting Information (SI).

Figure 1 shows the isotherms of σ and π_r versus $x_{2,b}$ for the three binary solutions. With an increase in $x_{2,b}$, σ gradually decreases and π_r gradually increases, showing the characteristics of conventional L-type isotherms [33]. Based on the modified Eberhart mixing rule [28], $\pi_r = \phi_{2,s}$, thus the π_r -isotherms are the isotherms of $\phi_{2,s}$ versus $x_{2,b}$. For the three binary solutions, their π_r isotherms are above the “ideal” correlation line (as marked with the dotted line), indicating the positive adsorption of component 2 occurs. This is reasonable due to $\sigma_2^0 < \sigma_1^0$ for the three systems. The π_r values at given $x_{2,b}$ increase in turn for DIM (1)–FA (2), DIM (1)–DMF (2), and FA (1)–DMF (2), indicating their adsorption trends increase in turn.

The $\pi_r - x_{2,b}$ data of the three binary solutions were linearly fitted using Equation (8), as shown in Figure 2. All of the plots of $\lg[\pi_r(1 - x_{2,b})/(1 - \pi_r)]$ versus $\lg x_{2,b}$ show good straight lines, with the adjusted coefficients of determination being 0.988, 0.995, and 0.993 for DIM–FA, DIM–DMF, and FA–DMF, respectively. From the slopes and intercepts of the plots, the n and K_x^* of the three solutions were estimated, and the K_x was then obtained, which are listed in Table 2, where the standard deviations of the best-fitted n and $\lg K_x^*$ values were less than 0.05 and 0.04, respectively. For all of the three systems, $K_x > 1$, corresponding to positive adsorption.

**Figure 1.** Cont.

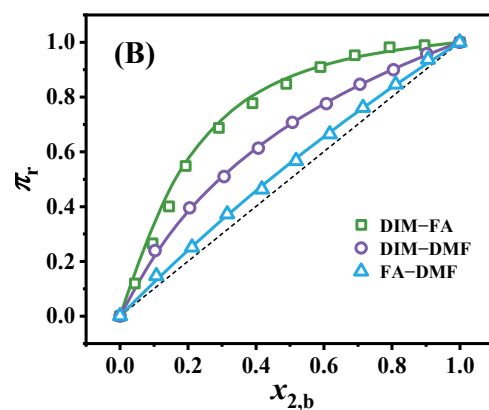


Figure 1. Isotherms of (A) σ and (B) π_r vs. $x_{2,b}$ for binary solutions. The symbols represent the experimental data, and the solid lines represent the fitting using the SAA model (Equations (6) and (7)). The dotted lines represent the “ideal” correlation.

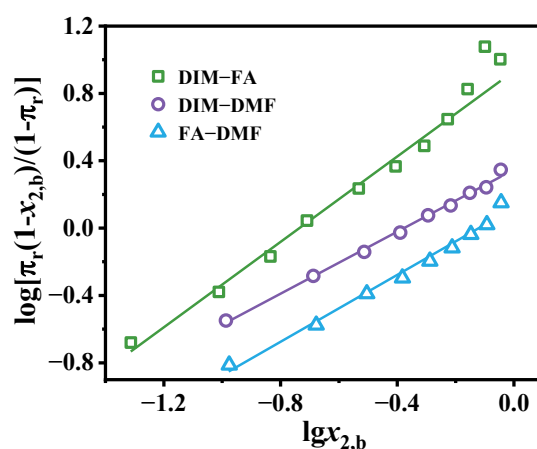


Figure 2. Linear fitting plots of Equation (8) for $\pi_r - x_{2,b}$ data of binary solutions. The symbols represent the experimental data, and the solid lines represent the fitting using the SAA model (Equation (8)).

Table 2. Best-fitting parameter values for surface tension data of binary solutions. (AAD and ARD correspond to the $\sigma - x_{2,b}$ data over the entire $x_{2,b}$ range).

Binary Solution	n	K_x^*	K_x	AAD (mN/m)	ARD (%)	ΔG_{ad}^0 (kJ/mol)
DIM (1)–FA (2)	1.27	8.45	6.37	0.059	0.13	−3.62
DIM (1)–DMF (2)	0.92	2.21	2.47	0.042	0.10	−2.44
FA (1)–DMF (2)	1.00	1.28	1.38	0.040	0.10	−0.80

The $\sigma - x_{2,b}$ and $\pi_r - x_{2,b}$ curves of the three binary solutions were then calculated using Equations (6) and (7), respectively, with the n and K_x^* values thus obtained (Table 2), which are also shown in Figure 1. All of the model curves coincide well with the experimental data. The AAD and ARD of the model-predicted σ values with the experimental ones are listed in Table 2, which are less than 0.06 mN/m and 0.15%, respectively. These results indicate that the SAA model is reasonable, which can well describe the σ or π_r -isotherms of the three binary solutions.

It should be noted that for DIM-DMF and FA-DMF systems, $K_x > 1$ and $n \leq 1$, consistent with the L-type isotherms intuitively observed [33]. However, for the DIM-FA system, $K_x > 1$ and $n > 1$, which actually correspond to the S-type isotherms [33], different from the L-type isotherm intuitively observed. This is because the negative deviation of

π_r from the ideal correlation line at extremely low $x_{2,b}$ ($x_{2,b} < 2.7 \times 10^{-3}$) is too small to appear on the figure. The $\pi_r - x_{2,b}$ data of the DIM-FA were also nonlinearly fitted using the Langmuir-like model (Equations (4) or (7) with $n = 1$), showing the best-fitted $K_x^* = 5.22$ (Figure S1). The AAD and ARD obtained by the Langmuir-like model for σ data were ca. 0.14 mN/m and 0.32%, respectively, which are larger than those obtained by the SAA model (0.059 mN/m and 0.13%, respectively). This indicates that the SAA model can better describe the σ or π_r -isotherms of the DIM-FA system than the Langmuir-like model (Figure S1).

In addition, the ΔG_{ad}^0 of the three systems at 25.0 °C was calculated using Equation (9) with the K_x and n values obtained, listed in Table 2. The ΔG_{ad}^0 values of the three systems are all negative, indicating that the surface adsorption is spontaneous. For DIM-FA, DIM-DMF, and FA-DMF, the absolute ΔG_{ad}^0 ($|\Delta G_{ad}^0|$) values decrease in turn, indicating the adsorption trends decrease in turn, consistent with their π_r -isotherms observed (Figure 1B).

3.2. The Surface Excess

The Gibbs excess Γ_2 values at different $x_{2,b}$ were calculated using the Gibbs-SAA equation (Equation (11)), as shown in Figure 3A. The change of Γ_2 with $x_{2,b}$ exhibits different trends for the three systems. For DIM-FA, with an increase in $x_{2,b}$, its Γ_2 initially increases and then decreases, showing a maximum at $x_{2,b} \approx 0.20$. This result is similar to those of binary aqueous solutions of short-chain alcohols [24,36,47]. For DIM-DMF, Γ_2 initially rapidly increases and then gradually reach equilibrium; while for FA-DMF, its Γ_2 continuously (almost linearly) increases. The shape of Γ_2 -isotherms is determined by K_x^* and n values. Owing to the fact that $d\Gamma_2/dx_{2,b} \geq 0$ at $x_{2,b} \rightarrow 0$, if $d\Gamma_2/dx_{2,b} \leq 0$ at $x_{2,b} \rightarrow 1$, a maximum Γ_2 will appear on the Γ_2 -isotherm. Therefore, it can be derived that only when $K_x^* \geq 2/(2n - 1)$ (or $K_x \geq 2v_{1,s}/[n(2n - 1)v_{2,s}]$), there exists a maximum on Γ_2 -isotherm. In addition, the $\Gamma_{2(x \rightarrow 1)}$ values of DIM-FA, DIM-DMF, and FA-DMF were obtained to be ca. 0.29, 2.23, and 2.09 $\mu\text{mol}/\text{m}^2$, which are listed in Table 3 for clarity.

Table 3. Adsorption parameters of binary solutions at 25 °C.

Binary Solution	$\Gamma_{2(x \rightarrow 1)}$ ($\mu\text{mol}/\text{m}^2$)	$\Delta\Phi_{2(x \rightarrow 1)}^{(1)}$	$\tau_{x \rightarrow 0}$ (nm)	$\tau_{x \rightarrow 1}$ (nm)	$N_{2(x \rightarrow 0)}$
DIM (1)–FA (2)	0.29	0.88	~0.8	0.05	1.2
DIM (1)–DMF (2)	2.23	0.56	0.78	0.69	1.2
FA (1)–DMF (2)	2.09	0.28	1.62	1.25	2.5

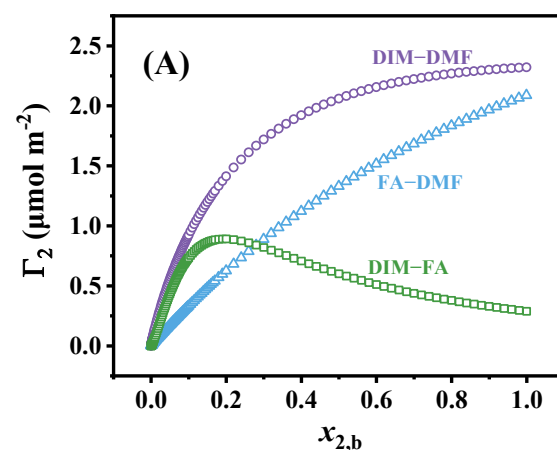


Figure 3. Cont.

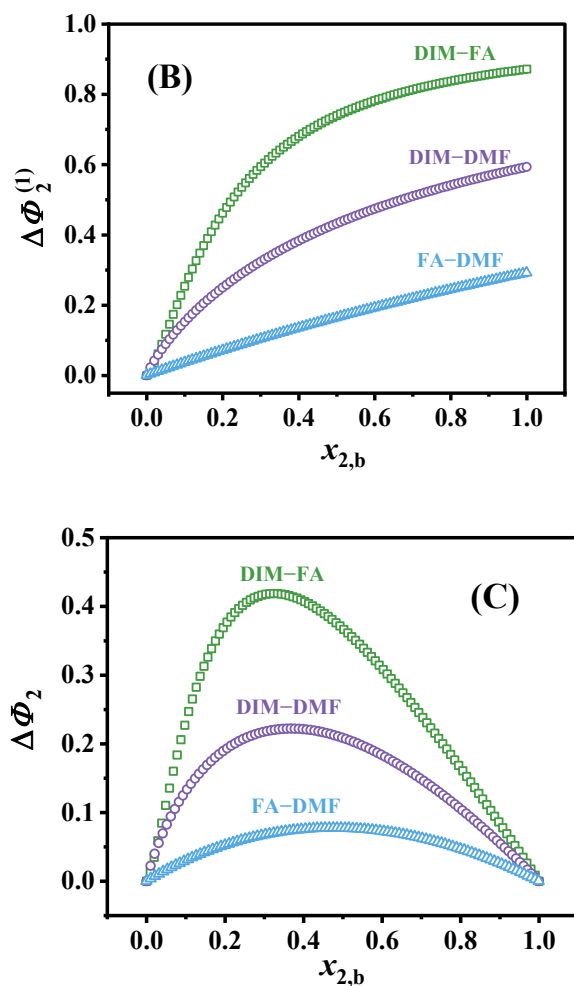


Figure 3. Changes in the Gibbs excesses (A) Γ_2 and (B) $\Delta\Phi_2^{(1)}$ and (C) the absolute surface excess $\Delta\Phi_2$ with bulk composition ($x_{2,b}$) for binary solutions.

The Gibbs surface excess $\Delta\Phi_2^{(1)}$ and the absolute surface excess $\Delta\Phi_2$ are also shown in Figure 3 (B and C) as a function of $x_{2,b}$. With an increase in $x_{2,b}$, $\Delta\Phi_2^{(1)}$ gradually increases. The $\Delta\Phi_{2(x \rightarrow 1)}^{(1)}$ values of DIM-FA, DIM-DMF, and FA-DMF were obtained to be ca. 0.88, 0.56, and 0.28, respectively, which are listed in Table 3. Large $\Delta\Phi_2^{(1)}$ corresponds to the strong adsorption trend. In addition, with an increase in $x_{2,b}$, $\Delta\Phi_2$ initially increases and then decreases, showing a maximum. At $x_{2,b} = 0$ and $x_{2,b} = 1$, $\Delta\Phi_2 = 0$, which is an expected result. The maximum $\Delta\Phi_2$ values of DIM-FA, DIM-DMF, and FA-DMF increases sequentially, corresponding to their increasing adsorption trends. $\Delta\Phi_2^{(1)}$ and $\Delta\Phi_2$ can well reflect the adsorption trend of binary solutions.

3.3. Adsorption Layer Thickness

It has been demonstrated that the molar volumes of components in the surface phase (v_s) are larger than those in the bulk phase (v_b) [13,48–51]. Many models were suggested to estimate v_s [48–50], and the Paquette model was chosen here, which was commonly used in the literature [13,48–51]. The Paquette model [48] can be written as

$$v_s = v_c^{3/5} v_b^{2/5} \quad (24)$$

where v_c is the critical molar volume. The so-obtained v_s values of pure liquids (v_s^0) involved here at 25 °C are shown in Table 1.

The change in τ with $x_{2,b}$ was calculated using the ALT equation (Equation (18)) for DIM (1)–FA (2), DIM (1)–DMF (2), and FA (1)–DMF (2) systems, as shown in Figure 4, where the partial molar volumes of component 2 in the surface phase are assumed to be equal to their molar volumes ($v_{2,s} = v_{2,s}^0$). Note that for the DIM–FA system with $n > 1$, negative τ will be obtained at $x_{2,b} < 4.3 \times 10^{-4}$, which is unreasonable, thus only the τ values at $x_{2,b} > 6 \times 10^{-3}$ are shown here. The three systems exhibit different trends. With an increase in $x_{2,b}$, for the DIM–FA system (with $n > 1$), its τ gradually decreases (or exponentially decays, with $x_{2,b}$ from 6×10^{-3} to 1), similar to the literature-reported results for aqueous solutions of short-chain alcohols [7,8,14,36]. For the FA–DMF system (with $n = 1$), its τ almost linearly decreases. However, for the DIM–DMF system (with $n < 1$), its τ initially sharply increases and then gradually decreases, showing a maximum at $x_{2,b} = 0.04$. Similar results were reported in the literature [13,17,18] for the water–ethanol solution. These results indicate that the binary solutions with $n < 1$ exhibit a maximum on the τ – $x_{2,b}$ isotherms.

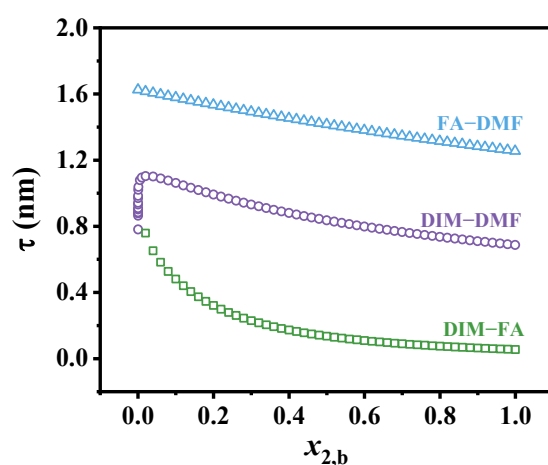


Figure 4. Change in surface adsorption layer thickness (τ) with bulk composition ($x_{2,b}$) for binary solutions.

In addition, except in the extremely low $x_{2,b}$ ($x_{2,b} \rightarrow 0$) range, the τ values of DIM–FA, DIM–DMF, and FA–DMF increase in turn, suggesting strong adsorption leads to a small τ . The τ values observed here for the three systems (at $x_{2,b} = 0.5$) are ca. 0.2–1.4 nm, which are comparable with those obtained by other models [13–15,18,52,53], molecular simulations [8,11,54,55], and experimental measurements [4,6,8,11,56–58] for various binary mixtures (0.25–1.7 nm).

The $\tau_{x \rightarrow 0}$ and $\tau_{x \rightarrow 1}$ of the three binary solutions were calculated using Equations (19)–(21), which are listed in Table 3. Note that the $\tau_{x \rightarrow 0}$ of the DIM–FA was obtained by extrapolation (or at $x_{2,b} \approx 6 \times 10^{-3}$). The so-obtained $\tau_{x \rightarrow 0}$ values are ca. 0.78–1.62 nm and the $\tau_{x \rightarrow 1}$ values (of DIM–DMF and FA–DMF) are ca. 0.69–1.25 nm, which are comparable with the thickness of surface layers reported for pure liquids (0.45–1.43 nm) [4,6,55,58]. Note that a small $\tau_{x \rightarrow 1}$ value was observed for DIM–FA (only ~0.05 nm), arising from its small $\Gamma_{2(x \rightarrow 1)}$ and large $\Delta\Phi_2^{(1)}$ (Table 3).

Taking the side-length of the equivalent cubes of molecules in the surface phase (l_s , calculated using v_s^0 , Table 1) as a measure of the molecular size, the number of molecular layers of component 2 in the surface phase at $x_{2,b} \rightarrow 0$, denoted as $N_{2(x \rightarrow 0)}$, was estimated using $N_{2(x \rightarrow 0)} = \tau_{(x \rightarrow 0)} / l_{2,s}$ to be 1.2, 1.2, and 2.5 for DIM–FA, DIM–DMF, and FA–DMF, respectively, which are listed in Table 3. The $N_{2(x \rightarrow 0)}$ values obtained here (ca. 1.2–2.5) suggest that the surface phase contains one to three molecular layers, which is close to those reported in the literature [4,6,13,16,26,52].

4. Conclusions

The surface tensions (σ) of binary solutions of DIM (1)–FA (2), DIM (1)–DMF (2), and FA (1)–DMF (2) were determined at 25 °C over the entire bulk composition range, and their surface adsorption behaviors were analyzed using the SAA model, the modified Eberhart model, and the Gibbs adsorption equation.

The SAA model combined with the modified Eberhart model can well describe the σ -isotherms of the three binary solutions. The surface adsorption trends of component 2 in DIM–FA, DIM–DMF, and FA–DMF decrease in turn. The change trends of the Gibbs excess Γ_2 and adsorption layer thickness τ with $x_{2,b}$ are dependent of the K_x^* or K_x and n values. With an increase in $x_{2,b}$, Γ_2 continuously increases when $K_x^* < 2/(2n - 1)$, while when $K_x^* \geq 2/(2n - 1)$, Γ_2 initially increases and then gradually decreases, showing a maximum on the Γ_2 -isotherm. When $n \geq 1$, τ gradually decreases with an increase in $x_{2,b}$, while when $n < 1$, τ initially increases and then decreases, showing a maximum on the τ -isotherm. With an increase in the adsorption trend (or $|\Delta G_{ad}^0|$), Γ_2 and τ decrease while $\Delta\Phi_2^{(1)}$ and $\Delta\Phi_2$ increase. This work provides a better understanding of the surface adsorption behavior of liquid mixtures.

Supplementary Materials: The following supporting information can be downloaded at: <https://www.mdpi.com/article/10.3390/colloids9050067/s1>, Table S1: Surface tensions and compositions of DIM(1)–FA(2) binary mixtures at 25.0 °C. Table S2: Surface tensions and compositions of DIM(1)–DMF(2) binary mixtures at 25.0 °C. Table S3: Surface tensions and compositions of FA(1)–DMF(2) binary mixtures at 25.0 °C. Figure S1: (A) Nonlinear fitting plot of the Langmuir-like model for π_r – $x_{2,b}$ data of DIM–FA, with the best-fitted $K_x^* = 5.22$; (B) The σ – $x_{2,b}$ curves of DIM–FA calculated using the Langmuir-like model (with $K_x^* = 5.22$), showing AAD ≈ 0.14 mN/m and ARD $\approx 0.32\%$.

Author Contributions: Conceptualization, W.H.; methodology, W.H. and N.D.; investigation, Z.H., N.D. and W.H.; writing—original draft preparation, Z.H., N.D. and W.H.; supervision, W.H.; project administration, W.H.; funding acquisition, W.H. and N.D. All authors have read and agreed to the published version of the manuscript.

Funding: This research was funded by the National Natural Science Foundation of China (No. 22272088) to W. Hou, the National Oil & Gas Major Project of China (No. 2025ZD1403200) to N. Du, and the Natural Science Foundation of Shandong Province (China, No. ZR2025MS229) to N. Du. We would like to acknowledge the technical support from Shandong University Structural Constituent and Physical Property Research Facilities.

Data Availability Statement: The raw data supporting the conclusions of this article will be made available by the authors on request.

Conflicts of Interest: The authors declare no conflicts of interest.

References

1. Marmur, A. Interfaces at equilibrium: A guide to fundamentals. *Adv. Colloid Interface Sci.* **2017**, *244*, 164–173. [CrossRef]
2. Kaptay, G. The chemical (not mechanical) paradigm of thermodynamics of colloid and interface science. *Adv. Colloid Interface Sci.* **2018**, *256*, 163–192. [CrossRef]
3. Kleinheins, J.; Shardt, N.; Haber, M.E.; Ferronato, C.; Nozière, B.; Peter, T.; Marcolli, C. Surface tension models for binary aqueous solutions: A review and intercomparison. *Phys. Chem. Chem. Phys.* **2023**, *25*, 11055–11074. [CrossRef] [PubMed]
4. Fellows, A.P.; Duque, Á.D.; Balos, V.; Lehmann, L.; Netz, R.R.; Wolf, M.; Thämer, M. Sum-frequency generation spectroscopy of aqueous interfaces: The role of depth and its impact on spectral interpretation. *J. Phys. Chem. C* **2024**, *128*, 20733–20750. [CrossRef]
5. Privat, M.; Bennes, R.; Tronel-Peyroz, E. Ellipsometry and adsorption: The determination of isotherms and the adsorbed layer thickness and fluctuations of the composition in the liquid-vapor interface. *J. Colloid Interface Sci.* **1988**, *121*, 198–207. [CrossRef]
6. Douillard, J.M. Experimental approach of the relation between surface tension and interfacial thickness of simple liquids. *J. Colloid Interface Sci.* **2009**, *337*, 307–310. [CrossRef] [PubMed]
7. Li, Z.X.; Lu, J.R.; Styrkas, D.A.; Thomas, R.K.; Rennie, A.R.; Penfold, J. The structure of the surface of ethanol/water mixtures. *Mol. Phys.* **1993**, *80*, 925–939. [CrossRef]

8. Hyde, A.E.; Ohshio, M.; Nguyen, C.V.; Yusa, S.I.; Yamada, N.L.; Phan, C.M. Surface properties of ethanol/water mixtures: Thickness and composition. *J. Mol. Liq.* **2019**, *290*, 111005. [\[CrossRef\]](#)
9. Raina, G.; Kulkarni, G.U.; Rao, C.N.R. Surface enrichment in alcohol–water mixtures. *J. Phys. Chem. A* **2001**, *105*, 10204–10207. [\[CrossRef\]](#)
10. Chen, H.; Gan, W.; Wu, B.H.; Wu, D.; Guo, Y.; Wang, H.F. Determination of structure and energetics for Gibbs surface adsorption layers of binary liquid mixture 1. Acetone + water. *J. Phys. Chem. B* **2005**, *109*, 8053–8063. [\[CrossRef\]](#)
11. Liu, J.; Li, X.; Hou, J.; Li, X.; Lu, Z. The influence of sodium iodide salt on the interfacial properties of aqueous methanol solution by a combined molecular simulation and sum frequency generation vibrational spectroscopy study. *Langmuir* **2019**, *35*, 7050–7059. [\[CrossRef\]](#)
12. Kirmse, K.; Morgner, H. Binary liquid mixtures. The relation between surface tension and surface composition as studied by mies (metastable induced electron spectroscopy). *Langmuir* **2006**, *22*, 2193–2199. [\[CrossRef\]](#)
13. Rafati, A.A.; Bagheri, A.; Khanchi, A.R.; Ghasemian, E.; Najafi, M. Application of the UNIFAC model for prediction of surface tension and thickness of the surface layer in the binary mixtures. *J. Colloid Interface Sci.* **2011**, *355*, 252–258. [\[CrossRef\]](#)
14. Azizian, S.; Moghadam, T.F. Derivation of a new equation for prediction of the thin layer depth of the extended-Langmuir model for dilute binary mixtures. *Colloids Surfaces A* **2011**, *378*, 67–71. [\[CrossRef\]](#)
15. Lemraski, E.G.; Pouyanfar, Z. Prediction of surface tension, surface mole fraction and thickness of the surface layer in the ionic liquid binary mixtures. *J. Mol. Liq.* **2015**, *203*, 52–58. [\[CrossRef\]](#)
16. Bermúdez-Salguero, C.; Gracia-Fadrique, J. Gibbs excess and the calculation of the absolute surface composition of liquid binary mixtures. *J. Phys. Chem. B* **2015**, *119*, 5598–5608. [\[CrossRef\]](#) [\[PubMed\]](#)
17. Bagheri, A.; Fazli, M.; Bakhshaei, M. Surface properties and surface thickness of aqueous solutions of alcohols. *J. Mol. Liq.* **2016**, *224*, 442–451. [\[CrossRef\]](#)
18. Santos, M.S.C.S.; Reis, J.C.R. Thermodynamic evaluation of molar surface area and thickness of water + ethanol mixtures. *J. Mol. Liq.* **2018**, *255*, 419–428. [\[CrossRef\]](#)
19. Hernández, A.; Tahery, R. Modeling of surface tension and phase equilibria for water + amine mixtures from (298.15 to 323.15) K using different thermodynamic models. *J. Solut. Chem.* **2022**, *51*, 31–57. [\[CrossRef\]](#)
20. Ma, W.; Du, N.; Hou, W. Predicting surface tension and surface composition of multicomponent liquid mixtures. (I) Ternary mixtures of isopropanol, water, and *n*-decane or *n*-tetradecane. *Chem. Phys.* **2025**, *595*, 112718. [\[CrossRef\]](#)
21. Jia, Q.; Du, N.; Deng, Q.; Hou, W. Effect of temperature on the surface aggregation adsorption of water–alcohol binary mixtures. *J. Mol. Liq.* **2025**, *431*, 127825. [\[CrossRef\]](#)
22. Gibbs, J.W. On the equilibrium of heterogeneous substances. *Trans. Conn. Acad. Arts Sci.* **1878**, *3*, 441–458. [\[CrossRef\]](#)
23. Butler, J.A.V. The thermodynamics of the surfaces of solutions. *Proc. R. Soc. London Ser. A* **1932**, *138*, 348–375.
24. Guggenheim, E.A.; Adam, N.K. The thermodynamics of adsorption at the surface of solutions. *Proc. R. Soc. London Ser. A* **1933**, *139*, 218–236.
25. Eberhart, J.G. The surface tension of binary liquid mixtures. *J. Phys. Chem.* **1966**, *70*, 1183–1186. [\[CrossRef\]](#)
26. Shereshefsky, J.L. A theory of surface tension of binary solutions I. Binary liquid mixtures of organic compounds. *J. Colloid Interface Sci.* **1967**, *24*, 317–321. [\[CrossRef\]](#)
27. Connors, K.A.; Wright, J.L. Dependence of surface tension on composition of binary aqueous-organic solutions. *Anal. Chem.* **1989**, *61*, 194–198. [\[CrossRef\]](#)
28. Laaksonen, A.; Kulmala, M. An explicit cluster model for binary nuclei in water–alcohol systems. *J. Chem. Phys.* **1991**, *95*, 6745–6748. [\[CrossRef\]](#)
29. Piñeiro, Á.; Brocos, P.; Amigo, A.; Gracia-Fadrique, J.; Lemus, M.G. Extended Langmuir isotherm for binary liquid mixtures. *Langmuir* **2001**, *17*, 4261–4266. [\[CrossRef\]](#)
30. Bermúdez-Salguero, C.; Clavijo-Penagos, J.A.; Romero, C.M.; Gracia-Fadrique, J. New insight into surface tension inverted curvature for liquid-liquid and solid-liquid binary mixtures: The special case of hexamethylenetetramine in water. *Colloid Surf. A* **2014**, *448*, 53–59. [\[CrossRef\]](#)
31. Phan, C.M. The surface tension and interfacial composition of water–ethanol mixture. *J. Mol. Liq.* **2021**, *342*, 117505. [\[CrossRef\]](#)
32. Phan, C.M. Affinity of amphiphilic molecules to air/water surface. *ACS Omega* **2023**, *8*, 47928–47937. [\[CrossRef\]](#)
33. Qi, W.; Yu, X.; Du, N.; Hou, W. General adsorption model to describe sigmoidal surface tension isotherms of binary liquid mixtures. *Langmuir* **2023**, *39*, 507–518. [\[CrossRef\]](#)
34. Qi, W.; Hou, W. A model for predicting the surface tension and composition of multicomponent liquid mixtures. *Sci. Sin. Chim.* **2023**, *53*, 1236–1246. [\[CrossRef\]](#)
35. Mulero, Á.; Hernández, A.; Vadillo-Rodríguez, V.; Cachadiña, I. Correlations of surface tension for mixtures of *n*-alkanes as a function of the composition: Applicability and performance analysis of existing models. *Phys. Chem. Chem. Phys.* **2025**, *27*, 12812–12836. [\[CrossRef\]](#) [\[PubMed\]](#)
36. Yu, X.; Qi, W.; Deng, Q.; Hou, W. Surface adsorption of water-alcohol binary solutions. *Chem. J. Chin. Univ.* **2023**, *44*, 20230316.

37. Belton, J.W.; Evans, M.G. Studies in the molecular forces involved in surface formation. II. The surface free energies of simple liquid mixtures. *Trans. Faraday Soc.* **1945**, *41*, 1–12. [\[CrossRef\]](#)
38. Ma, P. *Handbook of Basic Data of Petrochemical Industries*; Chemical Industry Press: Beijing, China, 1982.
39. Jańczuk, B.; Wójcik, W.; Zdziennicka, A. Determination of the components of the surface tension of some liquids from interfacial liquid-liquid tension measurements. *J. Colloid Interface Sci.* **1993**, *157*, 384–393. [\[CrossRef\]](#)
40. Balkenende, A.R.; van de Boogaard, H.J.A.P.; Scholten, M.; Willard, N.P. Evaluation of different approaches to assess the surface tension of low-energy solids by means of contact angle measurements. *Langmuir* **1998**, *14*, 5907–5912. [\[CrossRef\]](#)
41. Oosterlaken, B.M.; van den Bruinhorst, A.; de With, G. On the use of probe liquids for surface energy measurements. *Langmuir* **2023**, *39*, 16701–16711. [\[CrossRef\]](#)
42. Michaels, A.; Alexander, R.; Becker, C. Estimation of surface tensions. *Ind. Eng. Chem.* **1950**, *42*, 2332–2336. [\[CrossRef\]](#)
43. Lomba, L.; Giner, B.; Bandrés, I.; Lafuente, C.; Pino, M.R. Physicochemical properties of green solvents derived from biomass. *Green Chem.* **2011**, *13*, 2062–2070. [\[CrossRef\]](#)
44. Lomba, L.; Giner, B.; Lopéz, M.C.; Aldea, L.; Lafuente, C. Thermophysical properties of furfural compounds. *Chem. Eng. Data* **2014**, *59*, 329–338. [\[CrossRef\]](#)
45. Rafati, A.A.; Ghasemian, E.; Iloukhani, H. Surface tension and surface properties of binary mixtures of 1,4-dioxane or *N,N*-dimethyl formamide with *n*-alkyl acetates. *J. Chem. Eng. Data* **2009**, *54*, 3224–3228. [\[CrossRef\]](#)
46. Zhang, S.; Zhao, L.; Yue, X.; Li, B.; Zhang, J. Density, viscosity, surface tension and spectroscopic studies for the liquid mixture of tetraethylene glycol + *N,N*-dimethyl formamide at six temperatures. *J. Mol. Liq.* **2018**, *264*, 451–457. [\[CrossRef\]](#)
47. Yano, Y.F. Correlation between surface and bulk structures of alcohol-water mixtures. *J. Colloid Interface Sci.* **2005**, *284*, 255–259. [\[CrossRef\]](#)
48. Goldsack, D.E.; White, B.R. An iterative technique for calculating surface tensions of non-electrolyte solutions. *Can. J. Chem.* **1983**, *61*, 1725–1729. [\[CrossRef\]](#)
49. Tronel-Peyroz, E.; Douillard, J.M.; Tenebre, L.; Bennes, R.; Privat, M. Associated complex formation in the liquid-vapor interface: The water-ethanol and water-*tert*-butyl alcohol systems. *Langmuir* **1987**, *3*, 1027–1034. [\[CrossRef\]](#)
50. Nath, S. Surface tension of nonideal binary liquid mixtures as a function of composition. *J. Colloid Interface Sci.* **1999**, *209*, 116–122. [\[CrossRef\]](#) [\[PubMed\]](#)
51. Santos, M.S.C.S.; Reis, J.C.R. New thermodynamics for evaluating the surface-phase enrichment in the lower surface tension component. *ChemPhysChem* **2014**, *15*, 2834–2843. [\[CrossRef\]](#) [\[PubMed\]](#)
52. Tahery, R.; Modarress, H.; Satherley, J. Surface tension prediction and thermodynamic analysis of the surface for binary solutions. *Chem. Eng. Sci.* **2005**, *60*, 4935–4952. [\[CrossRef\]](#)
53. Randles, J.E.B.; Behr, B. Adsorption at liquid interfaces. I. Surface tension at the interface between a binary liquid mixture and its vapour. *J. Electroanal. Chem.* **1972**, *35*, 389–404. [\[CrossRef\]](#)
54. Azad, R.; Sharma, T.; Martin, D.; Daschakraborty, S.; Raj, R. Unraveling the surface activity of ethanol–water mixtures through experiments and molecular dynamics simulations. *Langmuir* **2024**, *40*, 17577–17589. [\[CrossRef\]](#) [\[PubMed\]](#)
55. AbouHaidar, R.; Bougueroua, S.; Duflot, D.; Gaigeot, M.-P.; Wyslouzil, B.; Toubin, C. Unraveling aqueous alcohol freezing: New theoretical tools from graph theory to extract molecular processes in MD simulations. *Faraday Discuss.* **2025**, *258*, 396–418. [\[CrossRef\]](#) [\[PubMed\]](#)
56. Li, Z.X.; Lu, J.R.; Thomas, R.K.; Penfold, J. Neutron reflection study of butanol and hexanol adsorbed at the surface of their aqueous solutions. *J. Chem. Soc. Faraday Trans.* **1996**, *92*, 565–572. [\[CrossRef\]](#)
57. Yano, Y.F. Surface structure of aqueous 2-butoxyethanol mixtures studied by x-ray reflection. *J. Chem. Phys.* **2002**, *116*, 8093–8096. [\[CrossRef\]](#)
58. Fellows, A.P.; Duque, Á.D.; Balos, V.; Lehmann, L.; Netz, R.R.; Wolf, M.; Thämer, M. How thick is the air–water interface? A direct experimental measurement of the decay length of the interfacial structural anisotropy. *Langmuir* **2024**, *40*, 18760–18772. [\[CrossRef\]](#)

Disclaimer/Publisher’s Note: The statements, opinions and data contained in all publications are solely those of the individual author(s) and contributor(s) and not of MDPI and/or the editor(s). MDPI and/or the editor(s) disclaim responsibility for any injury to people or property resulting from any ideas, methods, instructions or products referred to in the content.